Transverse effects in photorefractive ring resonators

J. Leonardy

Institute of Applied Physics, Darmstadt University of Technology, Hochschulstrasse 4a, 64289 Darmstadt, Germany

M. Belić

Institute of Applied Physics, Darmstadt University of Technology, Hochschulstrasse 4a, 64289 Darmstadt, Germany, and Institute of Physics, P.O. Box 57, 11001 Belgrade, Yugoslavia

F. Kaiser

Institute of Applied Physics, Darmstadt University of Technology, Hochschulstrasse 4a, 64289 Darmstadt, Germany

Received November 4, 1997; revised manuscript received March 4, 1998

Transverse effects in unidirectional and bidirectional photorefractive ring resonators with high Fresnel numbers are investigated numerically. The onset of transverse-mode competition, as well as symmetry-breaking intermittent instabilities, is observed as the cavity detuning is varied. Phase relations and frequency shifts in the intracavity field, in particular, antisymmetric response with respect to the frequency shift and cavity detuning, are considered. The buildup of ordered transverse patterns whose temporal dynamics are either periodic or chaotic is followed. The temporal evolution of chaotic mode oscillation is identified as a crisis-induced intermittency at a heteroclinic tangency. © 1998 Optical Society of America [S0740-3224(98)01806-2]

OCIS codes: 230.5750, 160.5320.

1. INTRODUCTION

Photorefractive (PR) rings hold promise for use in image processing,[1] beam cleanup,[2] optical storage, and computing.[3] Such applications envisage operation in parallel. It is natural to inquire about the transverse effects in PR rings. These effects have not been the subject to much theoretical interest. Attention has been confined mostly to unidirectional rings at low Fresnel numbers; in addition, rings are interesting for the study of transverse pattern formation and spatiotemporal (ST) mode dynamics.[4–6] It is in these systems that the first demonstration of periodic and chaotic mode alternation as well as of turbulence by means of optical defects was accomplished.[7]

A general theory of mode structure in rings was developed by Yariv and by Kwong *et al.*[2] and by Anderson and Saxena.[8] In these and in more-recent accounts,[4–6] plane-wave (PW) or empty-cavity truncated mode decompositions were used to describe the intracavity field. Our approach is different. We let the loaded cavity spontaneously build intracavity modes, supplying only the pump fields and the resonator and crystal parameters. We observe the intracavity field response to changes in these parameters.

Specifically, we are interested in the response at high Fresnel numbers, when PW or empty-cavity mode decompositions are inappropriate. In this case longitudinal modes become important, and we investigate simple cases in which mode competition becomes weakly turbulent through intermittence. We do not use a Fresnel number as the bifurcation parameter because it conveys information about the geometrical aspects of the cavity and plays a role similar to the aspect ratio in hydrodynamics. We choose cavity detuning as a more relevant bifurcation parameter.

Section 2 of this paper contains a description of the model. In Section 3 we discuss unidirectional rings, in Section 4 we discuss bidirectional rings, and in Section 5 we list our conclusions.

2. MODEL

The geometry of interest is presented in Fig. 1. Transverse analysis of both unidirectional and bidirectional rings is performed by a realistic numerical simulation. We let intracavity fields in the ring grow from a seed, using energy supplied by the pumps. The fields circulate clockwise and counterclockwise about the ring, and interact with each other and with the pumps within a PR crystal that is placed as an active intracavity element. A numerical code consists of two loops, one dealing with the resonator and the other dealing with wave mixing in the crystal. For simulation of the wave mixing process we use our numerical four-wave mixing (4WM) procedure,[9] which is nested in the resonator loop.

Wave equations that describe the 4WM process in PR crystals in the paraxial slowly varying envelope approximation are of the form

$$\partial_z A_1 + \beta \hat{K} \cdot \nabla A_1 + i\phi\nabla^2 A_1 = QA_4 - \alpha A_1, \qquad (1a)$$

$$\partial_z A_2 + \beta \hat{K} \cdot \nabla A_2 - i\phi\nabla^2 A_2 = \bar{Q}A_3 + \alpha A_2, \qquad (1b)$$

0740-3224/98/061714-12$15.00

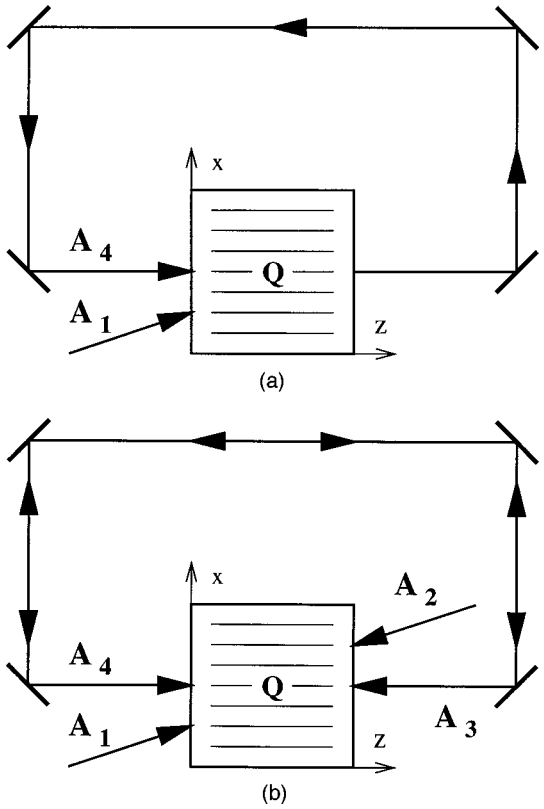

Fig. 1. Photorefractive ring oscillators: (a) unidirectional, (b) bidirectional. A_j are the slowly varying envelopes, and Q is the amplitude of the transmission grating.

$$\partial_z A_3 - \beta\hat{K} \cdot \nabla A_3 - i\phi\nabla^2 A_3 = -QA_2 + \alpha A_3, \tag{1c}$$

$$\partial_z A_4 - \beta\hat{K} \cdot \nabla A_4 + i\phi\nabla^2 A_4 = -\bar{Q}A_1 - \alpha A_4, \tag{1d}$$

where $A_j(x, y, z)$ are the slowly varying envelopes of the four beams, α is the linear absorption, β is the relative transverse displacement (caused by the noncollinear propagation of the four beams), and ϕ controls diffraction. In scaled coordinates $\beta = \theta/\Delta$, where θ is the half-angle at the beam intersection and Δ is the angular spread of the interacting beams. ϕ is proportional to the inverse of the Fresnel number: $\phi = (4\pi F)^{-1}$. $\hat{K} \cdot \nabla$ is the directional derivative in the transverse (x, y) plane along the gratings' unit wave vector $\hat{K}$, and ∇^2 is the transverse Laplacian. The propagation direction z is scaled by the crystal thickness d, and the transverse directions are scaled by the beam spot size w_0. We point $\hat{K}$ along the x axis.

The temporal evolution of the transmission grating amplitude Q is approximated by a relaxation-type equation:

$$\tau\partial_t Q + Q = \frac{\Gamma_0}{I}(A_1\bar{A}_4 + \bar{A}_2 A_3), \tag{2}$$

where τ is the relaxation time of the grating, Γ_0 is the PR coupling constant, and I is the total intensity. A more comprehensive theory[10,11] based on the Kukhtarev model[12] contains additional terms that incorporate transverse gradients of Q divided by the product of the Debye wave vector and the transverse beam spot size. This product is typically large, justifying the omission of spatial derivatives in Eq. (2). Such an approximation amounts to assuming that the characteristic length over which the grating amplitude changes in the transverse direction is large compared with the grating period. Inclusion of the spatial derivative terms renders a numerical analysis impractical.

The numerical solution of Eqs. (1) and (2) is accomplished by a modified spectral split-step method[13] that accounts for the two pairs of counterpropagating beams, Eqs. (1), and a Runge–Kutta-like method for the temporal evolution of Q, Eq. (2). Because of the adiabatic separation of the fast optical from the slow crystal processes, the spatial integration loop can be separated from, and nested within, the temporal integration loop.

The incident pump fields are displaced Gaussian beams:

$$A_1(x, y, z = 0) = C_1 G(-\xi; x - \beta/2, y), \tag{3a}$$

$$A_2(x, y, z = d) = C_2 G(\xi; x + \beta/2, y), \tag{3b}$$

where $z = 0$ and $z = d$ denote the entrance and the exit faces of the crystal, respectively, and $G(\xi; x, y)$ is the Gaussian beam function, where ξ is the curvature parameter. Pump fields A_1 and A_2 are kept constant in time. It is interesting to allow for the temporal variation of the pumps and monitor the changes in the intracavity field. An arrangement of this kind opens the possibility of interesting optical processing, such as optical logic or optical transistor action. An initial, PW analysis in this direction was undertaken in the research reported in Ref. 3.

Intracavity fields A_3 and A_4 are connected by the oscillation conditions

$$A_4(x, y, z = 0) = R\exp(ik_0 L)\mathrm{FSP}[A_4(x, y, z = d)], \tag{4a}$$

$$A_3(x, y, z = d) = R\exp(-ik_0 L)\mathrm{FSP}[A_3(x, y, z = 0)], \tag{4b}$$

where R represents passive resonator losses, $k_0 L$ is the total propagation phase shift (k_0 is the wave vector in free space and L is the total optical path length), and FSP is the free-space propagation operator, defined as

$$\mathrm{FSP}(A_{3/4}) = \mathrm{FT}^{-1}[\exp(\mp i\phi k^2 L/d)\mathrm{FT}(A_{3/4})], \tag{5}$$

where FT denotes the transverse spatial Fourier transform and FT^{-1} denotes its inverse. Initially amplitudes A_3 and A_4 are small, serving as mode seeds. Afterward they grow spontaneously as the intracavity fields. The spatial distribution of seeds has little influence on the final mode distribution. This distribution is determined by the resonator (including the crystal) and the pumps only. Even though the Fresnel number is large, the transverse-mode distribution need not be complicated, as it is strongly influenced by the Gaussian pumps. If $A_3 = A_4 = 0$ is assumed initially, it stays zero at all times. Likewise, by choosing $A_2 = A_3 = 0$ one obtains the two-wave mixing ring. The same numerical package allows for the analysis of both the unidirectional and the bidirectional rings.

Let us introduce the relevant variables and parameters. We present intracavity fields A_3 and A_4 at the en-

trance and the exit faces of the crystal as functions of cavity detuning Ψ_{ext}, defined as

$$k_0 L = 2M\pi + \Psi_{\text{ext}}, \tag{6}$$

with $-\pi \leqslant \Psi_{\text{ext}} \leqslant \pi$. M is an integer enumerating the longitudinal modes. The other relevant parameter is the imaginary part of the coupling constant, which we write as

$$\Gamma = \frac{\Gamma_0}{1 + i\tau\delta}, \tag{7}$$

where δ is the frequency-shift parameter. In the PW linear theory δ is equal to the (possibly) frequency offset Ω between the pump and the intracavity field. Here the situation is a bit different in that the linear relation between Ω and δ holds only in the region $\delta \approx 0$, where there is an appreciable wave interaction. Outside this band Ω saturates. We prefer δ as an independent control parameter, for its clear physical meaning and ease in controlling Γ. The imaginary part of Γ is responsible for the PR phase shift in the cavity.

To check numerics and compare it with the analytical and experimental results of Yeh[1] and Yariv and Kwong and of Kwong *et al.*,[2] we first treat the PW case. Figure 2 shows different longitudinal cavity resonances of intracavity field I_4 as functions of cavity detuning Ψ_{ext}. The coupling constant is kept real ($\delta = 0$). As Ψ_{ext} is swept through, a frequency offset Ω spontaneously appears in the phase of A_4, compensating for the cavity detuning. Figure 3 depicts one oscillation resonance for several gain coupling strengths. The frequency offset is the same for all Γ_0 values. Perfect agreement is found with Yeh.[1]

A similar Ω profile is obtained if the cavity is tuned ($\Psi_{\text{ext}} = 0$) and a sweep is performed through frequency-shift parameter δ (Fig. 4). A characteristic feature of a PW approximation is that a symmetric response of the intracavity field is found with respect to the cavity detuning (even-symmetric for the intensity and odd-symmetric for the frequency offset). The situation changes, however, if one varies the imaginary part of Γ at the same time. Figure 4 displays an asymmetric resonance profile and frequency offset with respect to the cavity detuning when $\delta \neq 0$. Such an asymmetric response has long been seen in experiment[2] but has not been explained.

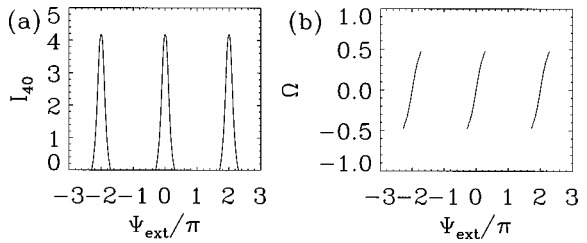

Fig. 2. (a) Intracavity intensity I_{40} as a function of cavity detuning Ψ_{ext}, for $\delta = 0$, $\Gamma_0 = 2$, and $R = 0.9$ and in the plane-wave case. The unit of intensity is the incident pump intensity. (b) Frequency offset Ω between the pump and the intracavity field as a function of cavity detuning Ψ_{ext}.

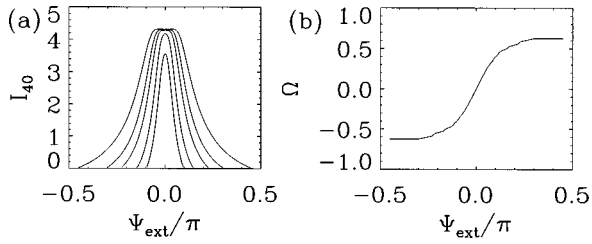

Fig. 3. Same as Fig. 2(a) but for different Γ_0 and across one resonance. The values of Γ_0 going from the inside to the outside profiles are 1, 2, 4, 6, and 10. (b) Same as Fig. 2(b).

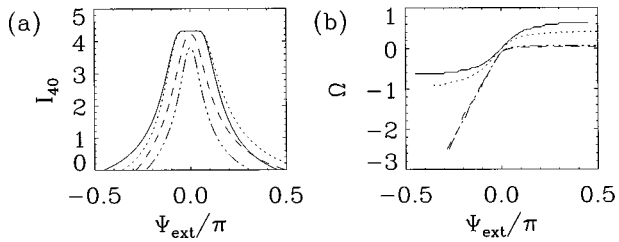

Fig. 4. (a) Same as Fig. 3(a) but for different $\tau\delta$ and for $\Gamma_0 = 10$. The values of $\tau\delta$ are as follows: solid curve, $\tau\delta = 0$; dotted curve, $\tau\delta = -0.03$; dashed curve, $\tau\delta = -0.47$; dashed–dotted curve, $\tau\delta = -0.8$. (b) Corresponding frequency offset Ω. The other parameters are as in Fig. 2.

3. TWO-WAVE MIXING UNIDIRECTIONAL RING

Experimental accounts of unidirectional rings abound;[2,4,5,7,14] however, theoretical accounts are few. Hennequin *et al.* and Dambly and Zeghlache[4] considered basic transverse dynamics when an external electric field is applied across the crystal. Arecchi and co-workers[7] have studied mode competition and optical turbulence in unidirectional rings in much detail. They were the first to present experimental evidence of optical phase defects in PR resonators. They also introduced the situation in which periodic and chaotic alternation of modes leads to ST chaos.

We proceed in the numerical treatment of the two-wave mixing ring by assuming that $A_2 = A_3 = 0$. The picture of mode buildup changes considerably with the inclusion of transverse dimensions. Here we include one transverse dimension, x. Under the influence of diffraction and nonlinear interaction within the crystal one expects different mode structures to arise in the transverse plane. The resonator can support a multitude of transverse and longitudinal modes. Within the resonator we place neither diffraction-limiting apertures nor curved mirrors. Of interest are those modes that spontaneously emerge, and their temporal evolution. We choose to present some results of mode competition and coexistence, and of spontaneous symmetry breaking in the cavity, which led to weak optical turbulence. An example of the transition to ST chaos through crisis-induced intermittency at a heteroclinic tangency is discussed.

Without frequency detuning ($\delta = 0$) one finds exclusively stationary solutions of the intensity for any value of Γ_0 and Ψ_{ext}. The intensity of the signal beam, $I_{40} = I_4(z = 0)$, attains a constant value, whereas the phase develops a frequency offset Ω from the pump, in agreement with the results obtained in the PW limit. The

beam profiles in the transverse dimension remain Gaussian. For the subsequent discussion we fix some parameters:

$$\Gamma_0 = 2.0, \qquad R = 0.9, \qquad \phi = 3 \times 10^{-4},$$

$$\alpha = 0.1, \qquad \beta = 0.$$

Note that we define ϕ by using the crystal thickness, and not the resonator length, as the scaling length in the propagation direction. The corresponding value of the Fresnel number is huge. We also set $L/d = 10$.

When a frequency detuning of $\delta = -0.47$ (in units of τ^{-1}) is present and the cavity detuning is in the range $-0.05\pi \leqslant \Psi_{\text{ext}} \leqslant 0.092\pi$, the situation is similar to the case when $\delta = 0$, and we observe a stationary Gaussian intensity profile. This structure is state 1 in Fig. 5, which displays a schematic overview of the bifurcation behavior that becomes different as Ψ_{ext} is further increased. Three additional transverse structures are observed, i.e., states $\bar{2}$, 3, and $\bar{4}$ in Fig. 5. The stationary intensity profiles of these states are shown in Fig. 6. For $\Psi_{\text{ext}} = 0.094\pi$ one observes a transverse beam profile consisting of two symmetric spots, resembling a Gauss–Hermite mode of the first order. For states 3 and $\bar{4}$ a bump and a dip emerge between the symmetric spots. Although I_{40} is constant in time, frequency detuning causes oscillation of the fields, similar to the one observed in the PW limit. Figure 7 displays the ST dynamics of the real part of A_{40} for all four states. The oscillation frequency Ω is different for each state, and it increases with increasing Ψ_{ext}. However, it remains less than one τ^{-1}. In Figs. 7(b) and 7(d) the real parts of the field reveal antisymmetry with respect to the beam center, and therefore we call them states $\bar{2}$ and $\bar{4}$, respectively. Their imaginary parts show identical, but 90° out of phase, oscillations.

Despite the fact that there are no specific criteria prescribed for the selection of transverse modes and that the Fresnel number is high, we observe low-order Gauss–Hermite mode structures as well as an alternating occurrence of symmetric and antisymmetric real and imaginary parts of field A_{40} with a higher mode index. They all arise spontaneously as Ψ_{ext} is varied. Cavity detuning acts as a mode selector, similar to that for lasers. In a laser with curved mirrors the Gauss–Hermite modes become resonant when the atomic transition frequency, the resonator detuning, or both are varied. In analogy, one might have a similar understanding of the occurrence of stationary structures observed in this system. Variation of Ψ_{ext} changes the oscillation frequency Ω of the signal beam; hence a resonance appears with the oscillation frequencies of different transverse-modelike structures; i.e., the frequency Ω that is supported by the resonator lies within the gain line of one of the stationary states. This state is favored and the others are suppressed. The difference between these structures and lasers is that the emission frequency in lasers remains close to the cavity resonance, whereas in unidirectional PR rings it remains close to the pump frequency. The gain bandwidth of PR rings is quite narrow.

Besides the occurrence of stationary transverse-modelike structures, we observe regular and irregular ST dynamics, depending on the value of Ψ_{ext} in between the

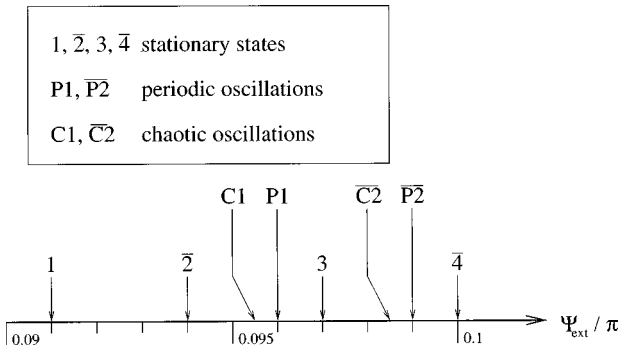

Fig. 5. Schematic representation of different ST states obtained by variation of cavity detuning Ψ_{ext}. The bars denote spatially antisymmetric states.

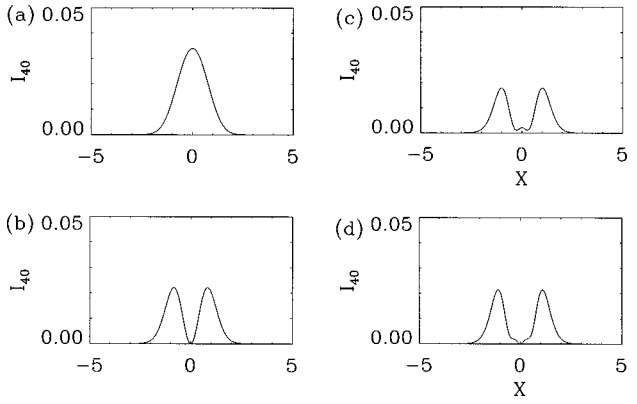

Fig. 6. Beam profiles of signal beam $I_{40} = I_2(x, z = 0)$: (a) state 1 ($\Psi_{\text{ext}} = 0.091\pi$), (b) state $\bar{2}$ ($\Psi_{\text{ext}} = 0.094\pi$), (c) state 3 ($\Psi_{\text{ext}} = 0.097\pi$), (d) state $\bar{4}$ ($\Psi_{\text{ext}} = 0.1\pi$).

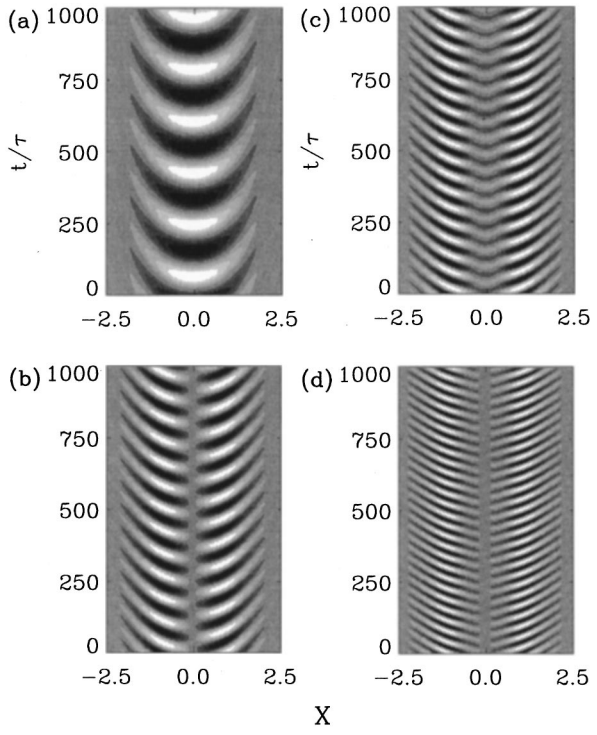

Fig. 7. ST dynamics of $\Re A_{40}$: (a)–(d) correspond to stationary states (a)–(d) in the same order in Fig. 6.

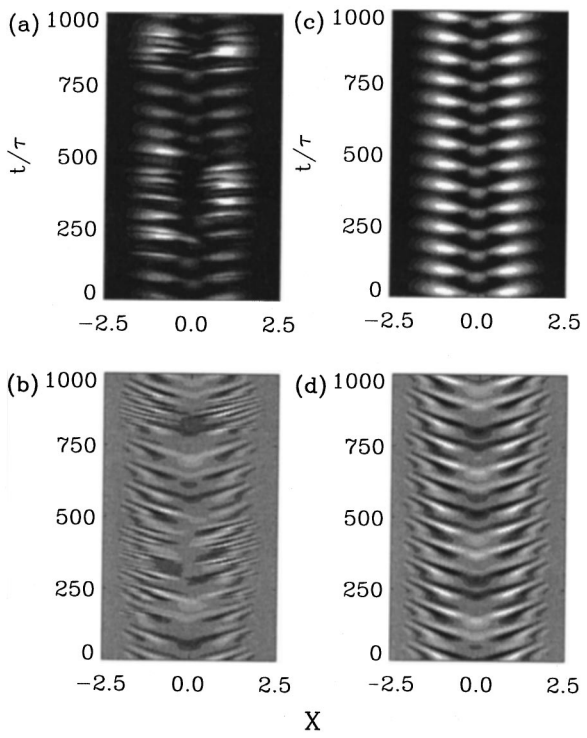

Fig. 8. Temporal change of the transverse profiles of intracavity field A_{40}: (a) intermittent chaotic state $C1$ for $\Psi_{ext} = 0.095\pi$, intensity distribution; (b) distribution of the real part; (c) periodic mode oscillation $P1$ for $\Psi_{ext} = 0.096\pi$, intensity distribution; (d) real-part distribution.

stationary states. When Ψ_{ext} is increased beyond state $\bar{2}$, chaotic oscillation ($C1$) followed by periodic oscillation ($P1$) occurs. Between symmetric state 3 and antisymmetric state $\bar{4}$ a spatially antisymmetric and temporally chaotic state $\bar{C}2$ and a periodic state $\bar{P}2$ are found. These periodic and chaotic states seem to be the superposition of two, not necessarily neighboring, stationary states. To illustrate this we have plotted in Fig. 8 the ST dynamics of chaotic state $C1$ and periodic state $P1$. In the intensity I_{40} of $P1$ the two lateral spots oscillate synchronously and alternately with a faint central spot. In the real part of A_{40} one sees two oscillating patterns: a symmetric pattern from state 3, as in Fig. 7(c), which is superimposed upon the symmetric pattern from state 1, as in Fig. 7(a). The power spectrum of state $P1$ [Fig. 9(b)] reveals two dominant frequency lines, which approximately coincide with frequencies Ω_1 and Ω_3 of the involved stationary state patterns 1 and 3. Other frequency lines in the spectrum are the higher harmonics of the frequency difference $\Omega_1 - \Omega_3$. This regular mode oscillation can therefore be understood as the phenomenon called mode beating.

Similar behavior holds for chaotic state $C1$, with some important differences. It is a symmetric state, as symmetric beating dominates the pattern. In the temporal signal one notes laminar sections that resemble state $P1$, and intermittent chaotic bursts. The intensity pattern consists of two spots plus one that oscillate alternately synchronously in the laminar regions and asynchronously in the irregular regions. During chaotic bursts a spontaneous symmetry breaking of the spatial transverse profile occurs. In the power spectrum of $C1$ [Fig. 9(a)] a broadband continous spectrum dominates. All these signatures point to weakly turbulent crisis-induced intermittency. The same analysis performed on states $\bar{P}2$ and $\bar{C}2$ yields similar results, the major difference being that one deals with the antisymmetric states.

By a Karhunen–Loève eigenmode analysis[15] we substantiated these findings. Such an analysis provides information about the ST behavior of involved substructures as well as about the symmetry of the substructural patterns.[16] In Fig. 10 the real and the imaginary parts (at the left) and the intensity (at the right) of the four largest eigenmodes $\mathbf{p}^{(i)}(x)$ of chaotic state $\bar{C}2$ are displayed. The first and third eigenmodes correspond to an antisymmetric, and the second and fourth eigenmodes to a symmetric, substructure. The intensities contain two or four prominent spots. The sum of the eigenvalues $\lambda^{(i)}$ of these four eigenmodes is larger than 95%, so these eigenmodes contain most of the information on the structure. The higher eigenmodes contribute small corrections.

The irregular temporal evolution of eigenmodes ($|a^{(i)}(t)|^2$) explains the dynamics of $\bar{C}2$ (Fig. 11). Eigenmode $|a^{(1)}(t)|^2$ performs a laminar (nearly periodic) oscillation in different time intervals, displaying synchronous oscillation of the two spots. Within such laminar inter-

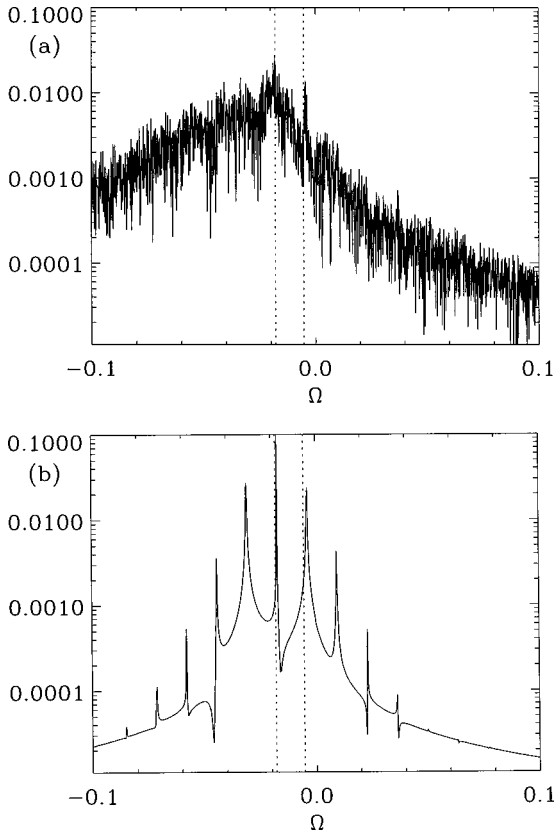

Fig. 9. (a) Power spectrum (arbitrary units) of chaotic state $C1$. The spectrum is calculated for the complex electric field $A_{40}(x = -0.74, t)$, and the frequency Ω is given in units of $1/\tau$. Dashed lines represent the frequencies of the stationary oscillation of states 1 ($\Omega_1 = -0.0053$) and 3 ($\Omega_3 = -0.018$). (b) Power spectrum of periodic oscillation $P1$.

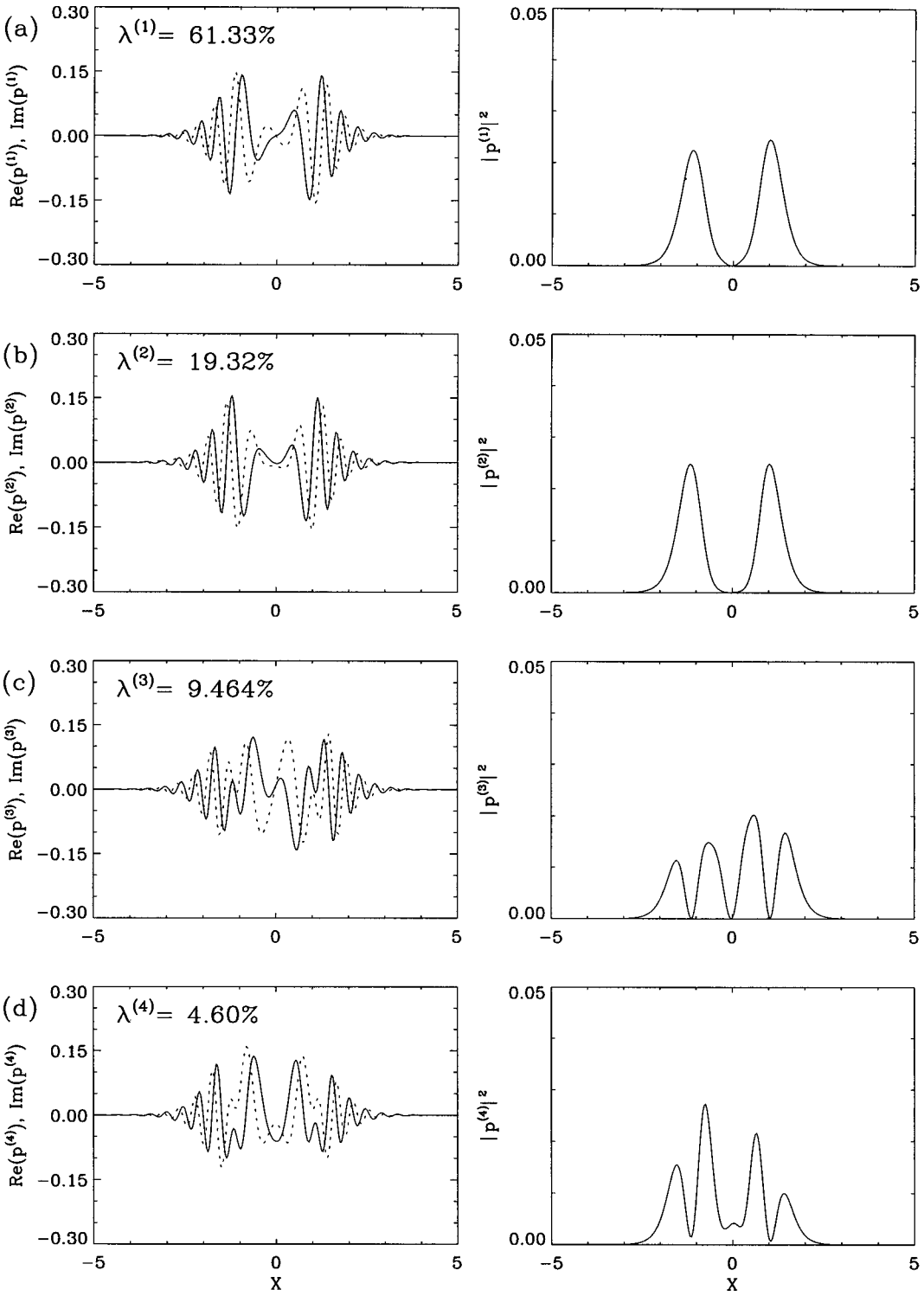

Fig. 10. Complex eigenmodes of chaotic oscillation $\bar{C}2$ in Fig. 6: left, real and imaginary parts of eigenmodes $\mathbf{p}^{(i)}(x)$; right, corresponding moduli $|\mathbf{p}^{(i)}|^2$.

vals the amplitude of oscillation increases, becomes irregular, and finally collapses. At that moment $|a^{(2)}(t)|^2$ emerges, and it lasts until another laminar interval begins. $|a^{(3)}(t)|^2$ exhibits an irregular temporal behavior; however, signal $|a^{(4)}(t)|^2$ is nearly synchronized with the bursts in $|a^{(2)}(t)|^2$. To characterize state $\bar{C}2$ further, we introduce a symmetry-breaking index S. It is defined as the integrated difference between the left and the right halves of the intensity profile.[17] If the two halves of the profile oscillate synchronously, then $S = 0$; if the oscillation is asynchronous, then $S \neq 0$. Thus S points to the appearence of spontaneous spatial symmetry breaking in the system. Figure 12(a) represents S for state $\bar{C}2$. It is seen that symmetry breaking in the system is connected to the appearence of eigenmodes $|a^{(2)}(t)|^2$ and $|a^{(4)}(t)|^2$. Eigenmode $|a^{(1)}(t)|^2$ is

nearly synchronous and antisymmetric, which justifies our denoting $\bar{C}2$ an antisymmetric, asynchronous chaotic state. There are also synchronous chaotic states in rings,[17] but they are not discussed here. An example of synchronous chaos is presented in Section 4. $\bar{P}2$ is an antisymmetric, synchronous periodic state.

The dynamic behavior of $\bar{C}2$ points toward a process called crisis-induced intermittency[18] as the route to ST chaos, which here is due to a boundary crisis. In the boundary crisis there is a heteroclinic tangency between two unstable solutions. For different time intervals the system oscillates in the basin of an unstable solution, represented in this case by $\mathbf{p}^{(1)}$. Following a heteroclinic tangential orbit, the system comes close to the basin of the other unstable orbit [here $\mathbf{p}^{(2)}$] and stays there for some time before again reaching the basin of attraction of

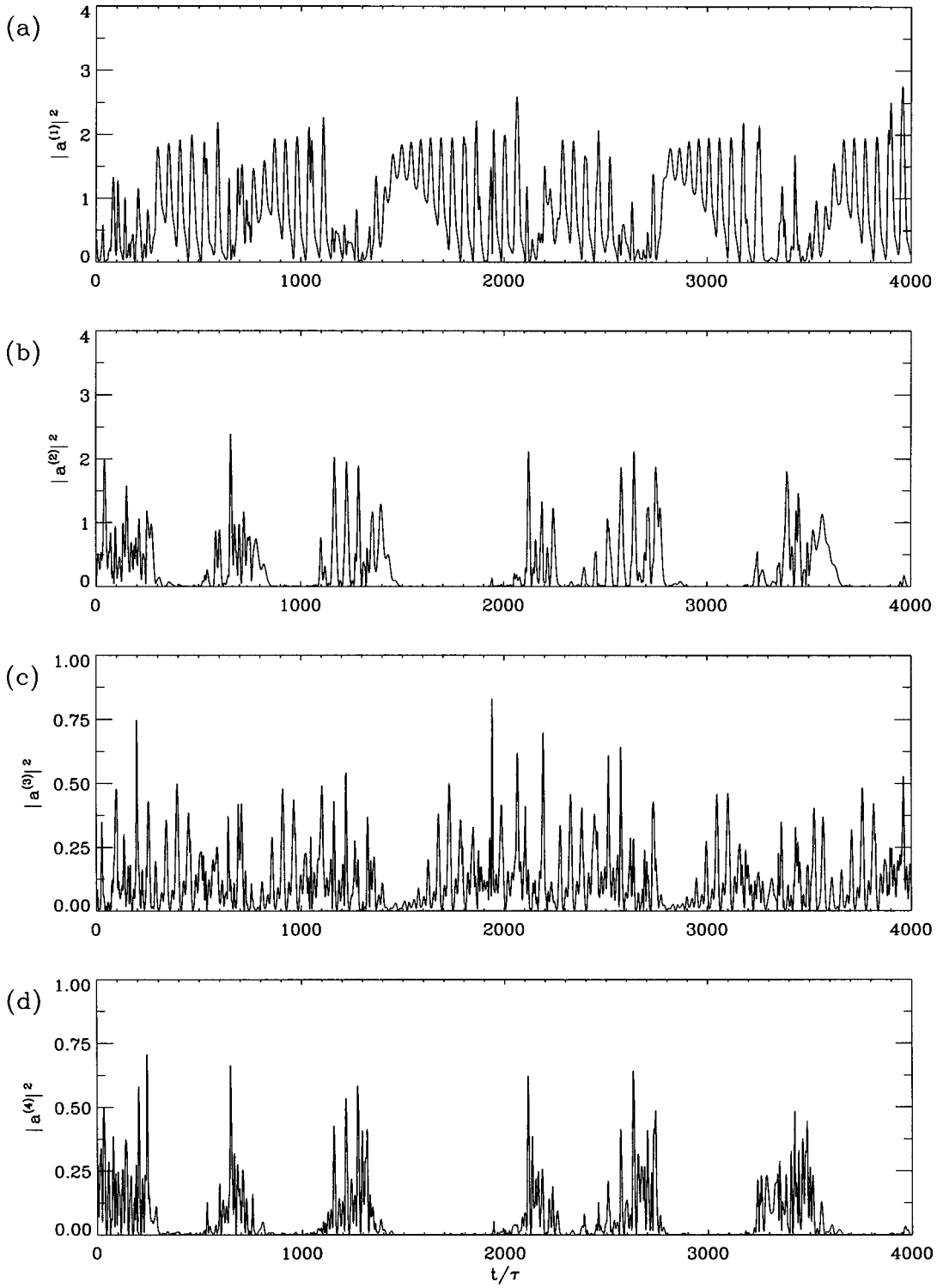

Fig. 11. Time expansion coefficients $|a^{(i)}|^2$ of the complex eigenmodes in Fig. 10.

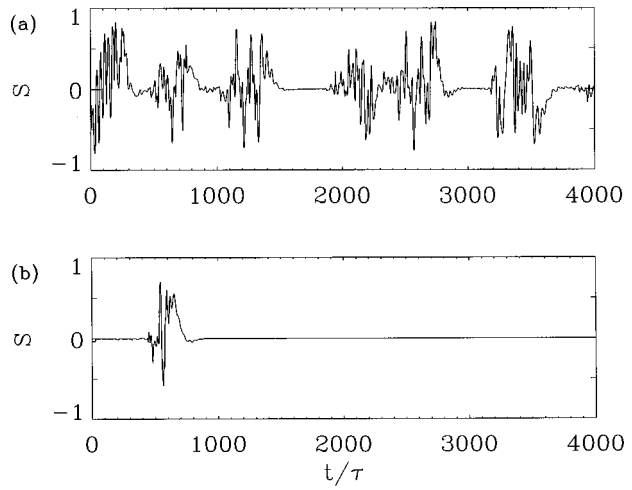

Fig. 12. Temporal development of symmetry-breaking index S: (a) state $\bar{C}2$, (b) state $\bar{P}2$.

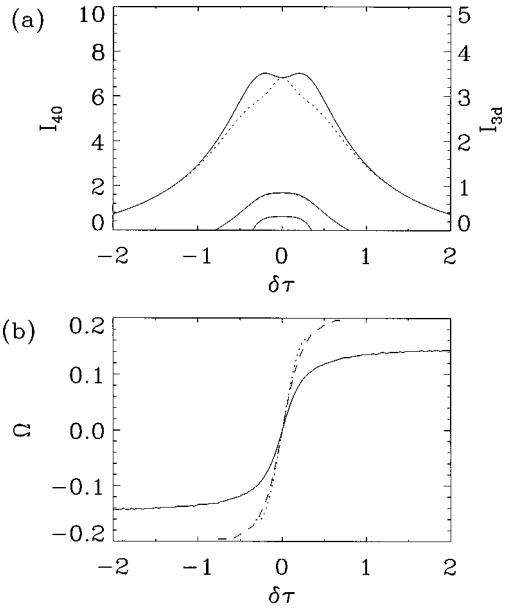

Fig. 13. (a) Integrated intracavity intensities I_{40} (solid curves) and I_{3d} (dashed curves) of the bidirectional ring as functions of frequency-shift parameter δ for three values of external mirror reflectivities R: 0.5, 0.7, 0.9 (from the inside to the outside). (b) Corresponding frequency offset Ω. The solid curve corresponds to the highest value of the reflectivity; the dotted curve, to the lowest.

the first orbit, and so on, with a temporally irregular repetition. Heteroclinic connections have already been suggested as the mechanism for mode alternation in unidirectional PR rings.[19] However, that theory is restricted to cylindrical symmetry and developed in terms of Gauss–Laguerre modes. We lack simple model expressions for the intracavity field. To identify this type of bifurcation as a crisis-induced intermittency it is necessary to investigate the dependence of the mean length $\langle \mathscr{L} \rangle$ of intervals with vanishing spatial symmetry breaking on bifurcation parameter Ψ_{ext}. This, however, would require much longer time series than the ones shown here. Even in the present form, our numerical simulations require massive computational support.

An important question pertaining to the buildup of intracavity field is whether it represents an oscillation or an optical amplification process. We believe that in essence the conclusions reached in our paper[20] on oscillation versus amplification in double phase conjugation stand in this case as well. Thus we believe that in the PW case both unidirectional and bidirectional rings are oscillators; in the transverse case they can be both oscillators and amplifiers, depending on the values of the diffractive ϕ and the convective β parameters. In addition to convection, an important mechanism in promoting amplifier be-

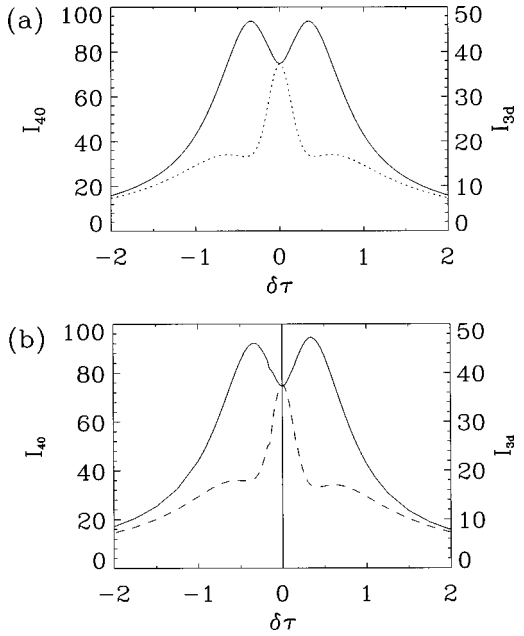

Fig. 14. (a) Integrated intracavity intensities I_{40} (solid curve) and I_{3d} (dashed curve) of the bidirectional ring as functions of frequency-shift parameter δ in the plane-wave case. (b) Same as (a) but for the transverse case.

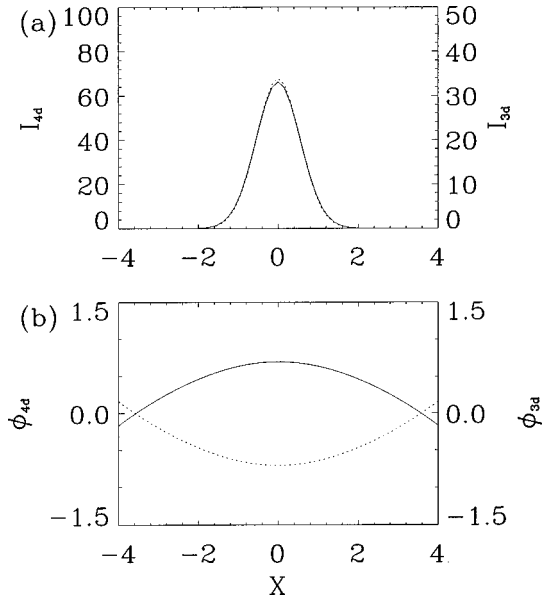

Fig. 15. (a) Transverse intensity profiles of intracavity intensities I_{4d} (solid curve) and I_{3d} (dashed curve) in the PC case. (b) Corresponding phases. Note the different scales for the intensities.

havior is the multimode operation of the device. Such devices exhibit a continuous buildup of modes over an extended threshold region.

4. FOUR-WAVE MIXING BIDIRECTIONAL RING

Plane-wave analysis of bidirectional rings has been performed by Gu and Yeh[21] and by Petrović and Belić.[22] Pattern dynamics in bidirectional PR rings has been numerically investigated by Chen and Abraham and by Chen *et al.*[6] In their analysis a truncated set of Gauss–Laguerre empty-cavity modes was used as the underlying modal basis, and the Fresnel number played the role of the bifurcation parameter. We use cavity detuning as the bifurcation parameter, as it acts as a mode selector. The Fresnel number acts more as an aspect ratio. We prefer to keep it fixed.

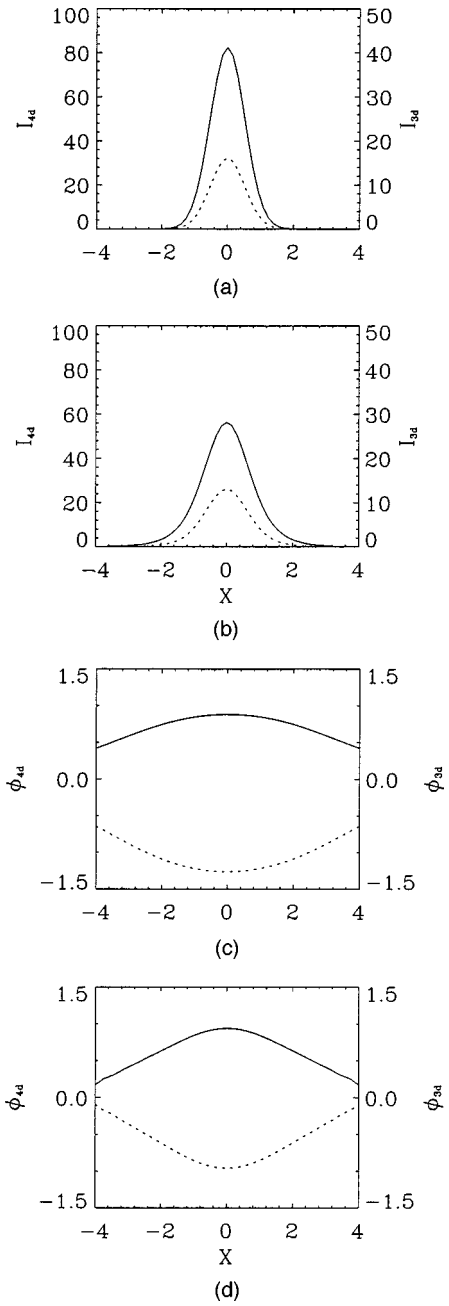

Fig. 16. (a) Same as Fig. 15, for $\tau\delta = -0.5$. (b) Same as (a), for $\tau\delta = 0.5$. Note the different scales for the intensities.

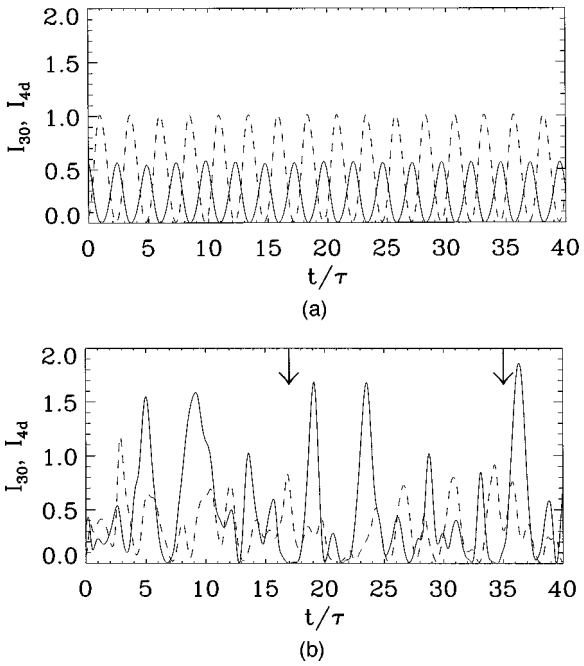

Fig. 17. Time signal at the center of beams I_{30} and I_{4d} when an external electric field is applied to the crystal: (a) $E_0 = 1.8$ kV/cm, periodic dynamics; (b) $E_0 = 3$ kV/cm, irregular dynamics. Arrows indicate the time interval during which the snapshots in Figs. 18(b) and 18(c) were taken.

In the 4WM rings the full set of Eqs. (1) and (2) must be used. We are again more interested in the antisymmetric response of the cavity with regard to the detuning and frequency shifts. A substantial difference in the operation of bidirectional rings, compared to that of unidirectional rings, is noted immediately. Both unidirectional and bidirectional rings require a coupling strength above a threshold for oscillation; however, only the unidirectional ring is self-starting. For small intensity ratios of pumps (less than 2), bidirectional rings require a nonzero seeding. A seeding threshold develops as well. A further difference is more consequential: Whereas the integrated intracavity intensity in the unidirectional ring is peaked at $\delta = 0$ and is flat topped at higher couplings, it develops a multipeaked structure in the bidirectional ring as the coupling strength increases. This phenomenon is visible in Fig. 13. The significance of this fact is that in a tuned cavity with $\Psi_{\text{ext}} = 0$ the unidirectional ring prefers to oscillate at the pump frequency, whereas the bidirectional ring will tend to detune spontaneously to maximize the 4WM efficiency. The physical origin of this spontaneous detuning is not fully understood and is the subject of some controversy.[23]

PW theory predicts the appearance of two symmetric peaks in intracavity intensity I_4 with respect to frequency parameter δ, whereas experimental results show two antisymmetric and shifted peaks. A discussion in the literature[23] aimed at explaining the discrepancy; no consensus was reached. We believe that simple mechanisms should be explored before more-exotic explanations are of-

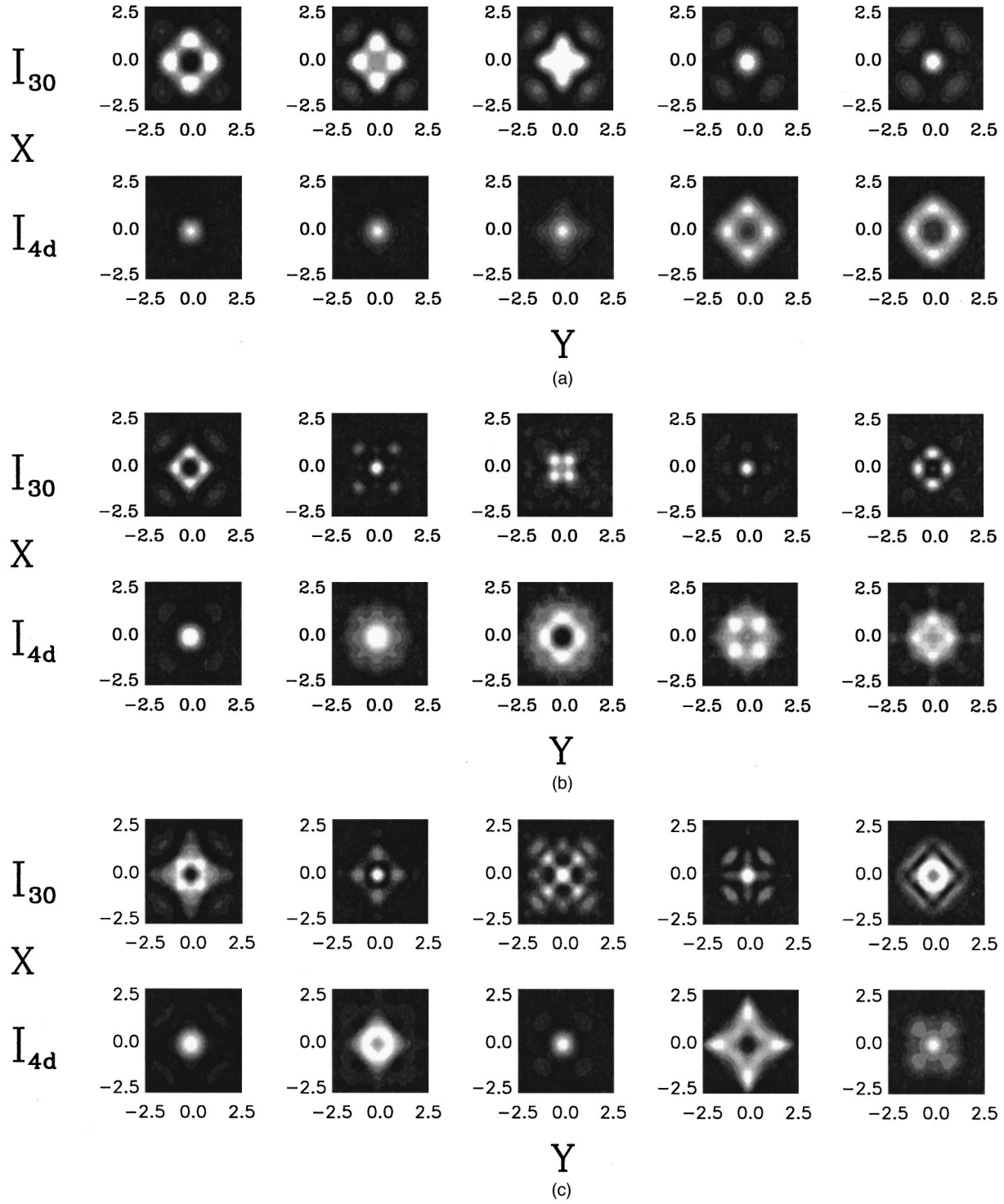

Fig. 18. Transverse patterns of intracavity intensities I_{30} and I_{4d}. (a) $E_0 = 1.8$ kV/cm, corresponding to Fig. 17(a). The snapshots were taken across one period, from $t = 11\tau$ to $t = 12.4\tau$. (b) $E_0 = 3$ kV/cm, corresponding to Fig. 17(b). (c) Continuation of (b). The time interval between two consecutive snapshots in (b) and (c) equals 2τ, starting from $t = 17\tau$.

fered. The simplest mechanism is to take into account the transverse spread of pumps and intracavity modes. Asymmetry obtained in this manner is depicted in Fig. 14.

When transverse dimensions are accounted for, the mode dynamics and the transition to ST chaos proceed similarly to those for the unidirectional rings. We are concerned here with two specific questions: First, under what conditions are the two counterpropagating cavity modes phase conjugates (PC's) of each other? It is known[6] that the PC property is not in general retained in the bidirectional ring; however it might be important with respect to the applications of rings. Second, bearing in mind the crucial influence of the crystal on mode selection

in the ring, what modelike structures can a crystal support by itself?

Figure 15 offers an answer to the first question. It displays transverse profiles of the intracavity modes, both the intensity and the phase distribution, for steady-state degenerate operation in a tuned cavity with real Γ_0 and away from instabilities. The pumps have the same Gaussian profile; both are focused into the crystal, with the beam ratio $r = |C_1/C_2|^2 = 2$. Under such symmetric conditions (except for r) the counterpropagating modes are PC's of each other. However, as soon as the system is disturbed with respect to degeneracy, cavity tuning, or both, the exact phase conjugation is lost. In Fig. 16 a nonzero frequency shift δ is introduced, which causes a significant change. Even though the phases of the modes are of the opposite sign, the modes are not PC's of each other, and the amplification factor of the ring is not the same for both of them.

Concerning the second question, we disconnect the crystal from the cavity and apply an external electric field across it. The field will play the role of the bifurcation parameter. Similar to the influence of δ, an external field makes the coupling constant complex, but in addition it makes the relaxation time of the crystal complex. Thus the oscillation is still frequency shifted. An external electric field also promotes instabilities of the intracavity field at higher Γ_0.[9,24] We now include both transverse dimensions. Figure 17 represents the temporal change of I_{30} and I_{4d} at the center of the beams for two values of the external field. The other parameters are as follows:

$$\Gamma_0 = 4.0, \qquad \phi = 0.01, \qquad \alpha = 0, \qquad \beta = 10^{-4}.$$

For $E_0 = 1.8$ kV/cm one obtains a periodic response; for $E_0 = 3$ kV/cm one obtains an irregular temporal response. It is interesting to note that in the periodic case the fields oscillate out of phase, which is reminiscent of the antiphase mode dynamics described theoretically in Ref. 6 and seen experimentally in Ref. 25. Figure 18 depicts transverse profiles of beams I_{30} and I_{4d} at the aforementioned two values of the external field. Antiphase dynamics is pronounced, even in the temporally chaotic case. Another interesting feature is that ordered, symmetric patterns are obtained, even though the fields at any spatial location within the crystal produce temporally chaotic signals. Such behavior is an example of the mode alternation with synchronized chaos.[7,17] We should mention that the square-symmetric patterns appear spontaneously, guided by the transverse wave-vector matching conditions appropriate for a 4WM process and by square mirrors. By imposing different matching conditions, and by depending on the boundary conditions, we can produce patterns of different (e.g., hexagonal) symmetry.

5. CONCLUSIONS

We have studied transverse effects in unidirectional and bidirectional PR ring resonators. In the case of the unidirectional ring oscillator, the occurrence of four different transverse structures similar to low-order Gauss–Hermite modes was observed, depending on the resonator detuning. These structures possess either symmetric or antisymmetric field distributions. Regular and irregular mode oscillations were found, which were shown to be a dynamic superposition of two modelike structures. Such superposition results in the appearence of two wandering spots (with or without an accompanying central peak), which have periodic and aperiodic motion. A complex eigenmode analysis allowed us to determine the symmetry of the complex spatial field modes. As far as the ST dynamics is concerned, apart from the periodic mode beating a heteroclinic tangency between symmetric and antisymmetric mode oscillation was observed, leading to ST chaos. The temporal evolution displayed the characteristic behavior of crisis-induced intermittency. Our numerical simulations are in general qualitative agreement with experimental results,[4,5,14] in which also superpositions of a few low-order Gauss–Hermite or Gauss–Laguerre modelike structures were found to dominate the ST dynamics of the intracavity field.

In the case of the bidirectional ring we investigated the possibility of the existence of PC intracavity modes. Under general oscillation conditions bidirectional rings do not support such modes. However, when the cavity is tuned, the coupling constant is real, and the pumps are PC's of each other, the counterpropagating intracavity modes will also be the PC's of each other. In view of the forbidding computational requirements for the full resonator simulation, we first investigated what modelike structures can be supported by an individual PR crystal. Such a question is relevant if one is aware of the crucial influence the crystal has on the selection of modes in PR resonators. A continuous variety of slowly evolving modelike transverse patterns was found, with spatially ordered intensity distributions and with either periodic or chaotic temporal evolution.

We plan to extend the simulations to two transverse dimensions in different PR resonators. We plan to consider the cases in which the pumps possess more-complicated spatial structure and are time varying. Such questions are more relevant for optical processing in parallel. The main obstacle to such a program is the need for massive computational support.

ACKNOWLEDGMENTS

Research at the Darmstadt University of Technology is supported within the SFB 185 project of the Deutsche Forschungsgemeinschaft. That at the Institute of Physics is supported by Project 01M07 of the Ministry of Science and Technology of the Republic of Serbia.

REFERENCES

1. P. Yeh, *Introduction to Photorefractive Nonlinear Optics* (Wiley, New York, 1993).
2. A. Yariv and S.-K. Kwong, Opt. Lett. **10**, 454 (1985); S.-K. Kwong, M. Cronin-Golomb, and A. Yariv, IEEE J. Quantum Electron. **QE-22**, 1508 (1986).
3. M. Petrović and M. R. Belić, Phys. Rev. A **52**, 671 (1995); M. Belić, Asian J. Phys. **4**, 53 (1995); M. Belić, M. Petrović, and F. Kaiser, Opt. Commun. **123**, 657 (1996).
4. D. Hennequin, L. Dambly, D. Dangoisse, and P. Glorieux, J.

Opt. Soc. Am. B **11**, 676 (1994); L. Dambly and H. Zeghlache, Phys. Rev. A **49**, 4043 (1994).
5. B. M. Jost and B. E. A. Saleh, J. Opt. Soc. Am. B **11**, 1864 (1994); Phys. Rev. A **51**, 1539 (1995).
6. Z. Chen and N. B. Abraham, Appl. Phys. B: **60**, 5183 (1995); Z. Chen, D. McGee, and N. B. Abraham, J. Opt. Soc. Am. B **13**, 1482 (1996).
7. F. T. Arecchi, G. Giacomelli, P. L. Ramazza, and S. Residori, Phys. Rev. Lett. **65**, 2531 (1990); **67**, 3749 (1991); F. T. Arecchi, Physica D **51**, 450 (1991).
8. D. Z. Anderson and R. Saxena, J. Opt. Soc. Am. B **4**, 164 (1987).
9. M. R. Belić, J. Leonardy, D. Timotijević, and F. Kaiser, Opt. Commun. **111**, 99 (1994); J. Opt. Soc. Am. B **12**, 1602 (1995).
10. A. A. Zozulya, G. Montemezzani, and D. Z. Anderson, Phys. Rev. A **52**, 4167 (1995).
11. F. T. Arecchi, S. Boccaletti, G. P. Puccioni, P. L. Ramazza, and S. Residori, Chaos **4**, 491 (1994).
12. N. V. Kukhtarev, V. B. Markov, S. G. Odulov, M. S. Soskin, and V. L. Vinetskii, Ferroelectrics **22**, 949 (1979).
13. M. Belić, "Some aspects of nonlinear interaction of light and matter," Ph.D. dissertation (City College of New York, New York, 1980; unpublished); J. Moloney, M. Belić, and H. M. Gibbs, Opt. Commun. **41**, 379 (1982); M. Lax, G. P. Agrawal, M. Belić, B. J. Coffey, and W. L. Louisell, J. Opt. Soc. Am. A **2**, 731 (1985).
14. S. R. Liu and G. Indebetouw, J. Opt. Soc. Am. B **9**, 1507 (1992); Opt. Commun. **101**, 442 (1993); D. Korwan and G. Indebetouw, Opt. Commun. **129**, 205 (1996); J. Opt. Soc. Am. B **13**, 1473 (1996).
15. R. Vautard and M. Ghil, Physica D **35**, 395 (1989); J. Leonardy, F. Kaiser, M. Belić, and O. Hess, Phys. Rev. A **53**, 4519 (1996).
16. M. Münkel, O. Hess, and F. Kaiser, "Stabilization of spatiotemporally chaotic semiconductor laser arrays by means of delayed optical feedback," Phys. Rev. E (to be published).
17. M. Sauer and F. Kaiser, Phys. Rev. E **54**, 2468 (1996).
18. C. Grebogi, E. Ott, F. Romeiras, and J. A. Yorke, Phys. Rev. A **36**, 5365 (1987).
19. F. T. Arecchi, S. Boccaletti, G. B. Mindlin, and C. Perez Garcia, Phys. Rev. Lett. **69**, 3723 (1992).
20. J. Leonardy, F. Kaiser, M. Belić, and D. Timotijević, Opt. Commun. **132**, 279 (1996).
21. C. Gu and P. Yeh, J. Opt. Soc. Am. B **8**, 1428 (1991).
22. M. Petrović and M. Belić, J. Opt. Soc. Am. B **12**, 1028 (1995).
23. M. R. MacDonald and J. Feinberg, Phys. Rev. Lett. **55**, 821 (1985); M. Cronin-Golomb and A. Yariv, Opt. Lett. **11**, 242 (1986); B. Fischer, S. Sternklar, and S. Weiss, IEEE J. Quantum Electron. **25**, 550 (1989); G. Pauliat, M. Ingold, and P. Gunter, IEEE J. Quantum Electron. **25**, 201 (1989).
24. J. Leonardy, F. Kaiser, M. Belić, and O. Hess, Phys. Rev. A **53**, 4519 (1996).
25. E. Lacot, F. Stoeckel, and M. Chenevier, Phys. Rev. A **49**, 3997 (1994); P. Mandel and J. Wang, Opt. Lett. **19**, 533 (1994).